

Recovered SN Ia rate from simulated LSST images

V. Petrecca^{*1,2}, M. T. Botticella¹, E. Cappellaro³, L. Greggio³, B. O. Sánchez⁴, A. Möller⁵, M. Sako⁶, M. L. Graham⁷, M. Paolillo^{2,1,8}, F. Bianco^{9,10}, and the LSST Dark Energy Science Collaboration

¹ INAF - Osservatorio Astronomico di Capodimonte, Salita Moiariello 16, 80131 Napoli, Italy

² Department of Physics, University of Napoli “Federico II”, via Cinthia 9, 80126 Napoli, Italy

³ INAF – Osservatorio Astronomico di Padova, Vicolo dell’Osservatorio 5, Padova 35122, Italy

⁴ Aix Marseille Univ, CNRS/IN2P3, CPPM, Marseille, France

⁵ Centre for Astrophysics and Supercomputing, Swinburne University of Technology, Mail Number H29, PO Box 218, 31122 Hawthorn, VIC, Australia

⁶ Department of Physics and Astronomy, University of Pennsylvania, Philadelphia, PA 19104, USA

⁷ DIRAC Institute, Department of Astronomy, University of Washington, 3910 15th Avenue NE, Seattle, WA 98195, USA

⁸ INFN — Sezione di Napoli, via Cinthia 9, 80126, Napoli, Italy

⁹ University of Delaware, 210 South College Ave., Newark, DE 19716, USA

¹⁰ Vera C. Rubin Observatory, Tucson, AZ 85719, USA

Received 19 December 2023 / Accepted 23 February 2024

ABSTRACT

Aims. The Vera C. Rubin Observatory’s Legacy Survey of Space and Time (LSST) will revolutionize Time Domain Astronomy by detecting millions of different transients. In particular, it is expected to increment the number of type Ia supernovae (SN Ia) of a factor of 100 compared to existing samples up to redshift ~ 1.2 . Such a high number of events will dramatically reduce statistical uncertainties in the analysis of SN Ia properties and rates. However, the impact of all other sources of uncertainty on the measurement of the SN Ia rate must still be evaluated. The comprehension and reduction of such uncertainties will be fundamental both for cosmology and stellar evolution studies, as measuring the SN Ia rate can put constraints on the evolutionary scenarios of different SN Ia progenitors.

Methods. We use simulated data from the Dark Energy Science Collaboration (DESC) Data Challenge 2 (DC2) and LSST Data Preview 0 to measure the SN Ia rate on a 15 deg^2 region of the Wide-Fast-Deep area. We select a sample of SN candidates detected on difference images, associate them to the host galaxy with a specially developed algorithm, and retrieve their photometric redshifts. Then, we test different light curves classification methods, with and without redshift priors (albeit ignoring contamination from other transients, as DC2 contains only SN Ia). We discuss how the distribution in redshift measured for the SN candidates changes according to the selected host galaxy and redshift estimate.

Results. We measure the SN Ia rate analyzing the impact of uncertainties due to photometric redshift, host galaxy association and classification on the distribution in redshift of the starting sample. We found a 17% average lost fraction of SN Ia with respect to the simulated sample. As 10% of the bias is due to the uncertainty on the photometric redshift alone (which also affects classification when used as a prior), it results to be the major source of uncertainty. We discuss possible reduction of the errors in the measurement of the SN Ia rate, including synergies with other surveys, which may help using the rate to discriminate different progenitor models.

Key words. Stars: supernovae – Galaxies: stellar content: surveys

1. Introduction

Type Ia supernovae (SN Ia) are violent explosions characterized by a peak in luminosity correlated to the duration of the event, which makes them standardizable candles (Phillips 1993; Tripp & Branch 1999) and fundamental cosmological probes (Riess et al. 1998; Perlmutter et al. 1999). There is general consensus that SN Ia are the result of a thermonuclear explosion of a carbon-oxygen White Dwarf (WD) with two possible progenitor channels: a WD accreting mass from a non-degenerate star (single degenerate scenario SD; Whelan & Iben 1973) or two WD spiraling together and eventually merging (double degenerate scenario DD; Webbink 1984; Iben & Tutukov 1984). However, the exact nature of their progenitors and the details of the explosion mechanism are not yet clear (see Livio & Mazzali 2018 for a recent review). Direct observations of both pre- and post-

explosion images do not provide unambiguous evidence for either SN Ia progenitor systems (e.g., Kelly et al. 2014; Graur & Woods 2019), or surviving companions (e.g., Schaefer & Pagnotta 2012; Kerzendorf et al. 2019). Similarly, detailed spectral analyses of SN Ia and their remnants are not able to clearly identify the companion star in the binary system (e.g., Badenes et al. 2007; Foley et al. 2012; Dhawan et al. 2016). The diversity of the SN Ia light curves and their correlation with the host galaxy properties are also not able to exclude any progenitor scenario, hence both of them might be at play.

An alternative way of putting constraints on the SN Ia progenitors system is the analysis of the delay times distribution (DTD), which is the time between the formation of the binary system and the SN Ia explosion. Different progenitor scenarios imply a different DTD from population synthesis models (Wang & Han 2012). As the SN Ia rate results from the convolution of the host galaxy star formation rate (SFR) and the DTD (Greggio 2005; Greggio 2010), measuring the SN Ia rate and the SFR for

* vincenzo.petrecca@inaf.it

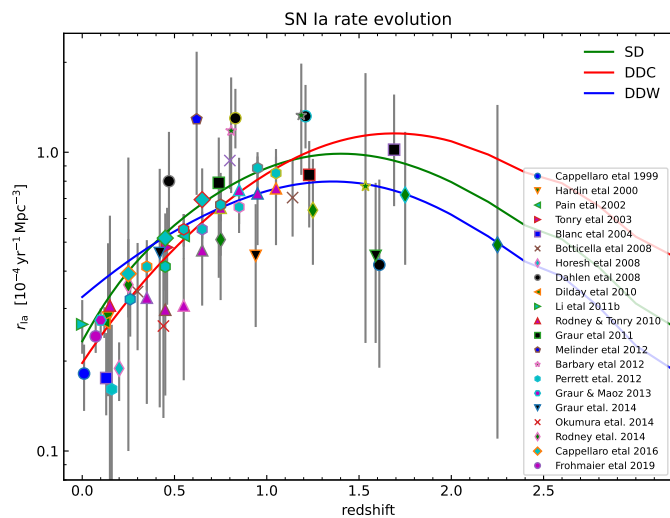


Fig. 1. Observed SN Ia rate as a function of redshift for different surveys, along with rate predictions for progenitor models from Greggio (2005): Single Degenerate (SD), Double Degenerate Close (DDC), Double Degenerate Wide (DDW).

a sample of galaxies is thus an empirical way of testing the DTD from different progenitor models (Maoz et al. 2012; Greggio & Cappellaro 2019; Strolger et al. 2020; Wiseman et al. 2021). More into detail, the SN Ia rate at a time t , $r_{SN Ia}(t)$ can be expressed as:

$$r_{SN Ia}(t) = k_{Ia} \int_0^t \psi(t - t_D) f_{Ia}(t_D) dt_D, \quad (1)$$

where k_{Ia} is the total number of SN Ia provided by a stellar population of unitary mass, ψ is the SFR, f_{Ia} is the DTD, and t_D is the delay time. Knowing the average cosmic star formation history (SFH) and the DTD for each progenitor system model, it is also possible to calculate the expected volumetric rate of SN Ia as a function of redshift and compare it with the observed rate.

Figure 1 shows the measurements of the SN Ia rate as a function of redshift from different surveys, along with rate predictions for DTD progenitor models from Greggio (2005), adopting the estimates of cosmic SFH from Madau & Fragos (2017). Theoretical rates have been normalized using the same $k_{Ia} = 0.8 \times 10^{-3} M_{\odot}^{-1}$ for all the models. The significant scatter between rate measurements from different surveys, as well as present day statistical and systematic uncertainties on each single measurement, do not allow us to distinguish between different progenitor models. Moreover, the theoretical predictions run quite close in the intermediate range $0.2 \lesssim z \lesssim 1.0$, making it difficult to discriminate among the different options. Greggio & Cappellaro (2019) show that measuring the SN Ia rate as a function of host galaxy intrinsic colors or specific SFR is more efficient in separating the predictions of different models, but data are only limited to the local Universe. Upcoming surveys, such as the Vera C. Rubin Observatory’s Legacy Survey of Space and Time (LSST;¹ Ivezić et al. 2019), may completely change the scenario. Indeed LSST will detect an enormous number of events in galaxies with a large range of different properties, strongly improving on both statistical and systematic uncertainties. Besides, having data from the same survey, with known and homogeneous properties, will also reduce the scatter between rate

measurements in different redshift and intrinsic color bins, compared to those coming from the combination of multiple surveys. While a dramatic reduction of statistical uncertainties will be easily attained by LSST, the actual effect of all other possible sources of uncertainty deserves a detailed analysis. Some of the uncertainties are not directly related to the survey and depend on the adopted software/criterion for the analysis (e.g., photometric redshift, transient classification) and the wealth of ancillary data (e.g., spectroscopic information).

In this work, we will assess the impact of uncertainties on the SN Ia rate using a simulation of the first 5 years of LSST. As the simulation does not include other SN types nor any correlation between the transients and the host galaxy properties, we only focus on evaluating the impact of uncertainties on the SN Ia rate as a function of redshift due to i) host galaxy association, ii) photometric redshift, iii) and light curves classification, using a sample of SN Ia detected on difference images (see Sect. 3). These sources of uncertainty, affecting the choice of the SN Ia sample and their host galaxies, also reflect on rate measurements as a function of specific SFR or intrinsic galaxy colors from spectral energy distribution (SED) fitting. Furthermore, the sources of error studied in this work are common in all transients studies, and understanding how they propagate in a final statistical analysis would be important for most of Time Domain science with LSST. Measuring the SN rate and shedding light on the evolutionary channels for SNe are also goals outlined in both Dark Energy Science Collaboration² (DESC) and Transient and Variable Stars Science Collaboration³ (TVSSC) roadmaps⁴ (Hambleton et al. 2023). The comprehension of all possible biases affecting the final measurement is thus a crucial point before the beginning of the survey. A more thorough investigation on the SN Ia rate from LSST as a tool to discriminate between progenitor models is left to subsequent analysis.

This paper is organized as follows. Section 2 provides a short summary of the LSST strategy and design. In Sect. 3 we briefly describe the simulation and the SN sample used in our analysis. In Sect. 4, we describe the procedure of association of transients to the host galaxies, and in Sect. 5 the photometric redshifts of the hosts. Section 6 is dedicated to the classification of light curves and the comparison of different approaches. Finally, we present the final measurement of the SN Ia rate in Sect. 7, comparing the results with the input of the simulation and providing quantitative estimates of different sources of uncertainty. In Sect. 8, we summarize our results and discuss future perspectives.

2. Rubin Observatory’s LSST

The LSST, expected to start in 2025⁵, will revolutionize Time Domain astronomy by imaging the entire southern sky every few nights for 10 years (Ivezić et al. 2019). It will be executed with the 8.4 m (6.7 m effective) Simonyi Telescope and a 3.2 gigapixel camera yielding a 9.6 deg^2 field of view. The instrument is equipped with 6 filters *ugrizy* and is expected to have a 5σ *r*-band magnitude depth of ~ 24.5 in a single 30 seconds visit and ~ 27.8 in the full stacked data. The survey design will enable to cover a wide range of science goals (LSST Science Collaboration et al. 2009). The main ones are i) exploring the transient and variable sky, ii) studying the dynamics of solar system objects,

² lsstdesc.org

³ lsst-tvssc.github.io

⁴ DESC roadmap: lsstdesc.org/assets/pdf/docs/DESC_SRM_latest.pdf

⁵ lsst.org/about/project-status

¹ lsst.org

iii) probing dark energy and dark matter, iv) and mapping the Milky Way. Fulfilling most of these science goals requires scanning the sky deep, wide and fast. Albeit the exact survey strategy is not yet defined, about 90% of the observing time will be devoted to the baseline wide-fast-deep (WFD) survey mode. The remaining 10% will be used to obtain improved coverage and cadence for specific regions, called deep drilling fields (DDF).

The exploration of the changing universe will be boosted by the implementation of difference image analysis (DIA; [Alard & Lupton 1998](#)) on the entire dataset. This technique consists of producing deep co-added images (templates) to be subtracted from each science observation in the same region of sky. Before the subtraction, the template is re-sampled to the pixel coordinate system of the new image and is convolved with a kernel matching their Point Spread Functions (PSFs). Variable sources are considered to be detected if they have a signal-to-noise ratio (S/N) greater than a threshold value (i.e., five for Rubin data products) on the resulting difference image. For each detected transient, LSST will issue an *alert* within 60 seconds of the end of the visit (defined as the end of image readout from the camera) to enable immediate follow-up observations with other facilities.

LSST is expected to process $\sim 10^5$ transient detections per night⁶ ([Ivezić et al. 2019](#); [Graham et al. 2020](#)). This includes SN Ia for which we expect an increment of a factor of 100 compared to existing samples up to redshift $z \sim 1.2$ (e.g., [Betoule et al. 2014](#); [Sako et al. 2018](#); [Jones et al. 2019](#)). Such a high number of events will dramatically reduce statistical uncertainties in the analysis of SN Ia properties and rates, which will be important both for cosmology and stellar evolution studies. The analysis of SNe is then expected to be only limited by the adopted observing strategy (affecting the sampling of light curves and the resulting classification of transients) and different sources of uncertainty, namely detection efficiency on difference images, photometric calibrations, artifact contamination levels, reliability of photometric redshifts of the host galaxies (e.g., precision, accuracy and fraction of catastrophic errors), efficiency of host galaxy association and photometric classification algorithms. Many of these aspects have been thoroughly looked into by recent works: [Sánchez et al. \(2022\)](#) measured detection efficiency, magnitude limits and photometric biases; [Alves et al. \(2022\)](#) and [Graham et al. \(2018\)](#) focused on the impact of different observing cadences on the classification of SNe and the reliability of photometric redshifts; [Schmidt et al. \(2020\)](#) compared different algorithms for photometric redshifts; the Photometric LSST Astronomical Time-series Classification Challenge (PLAsTiCC; [The PLAsTiCC team et al. 2018](#); [Kessler et al. 2019](#)) and its extension ELAsTiCC⁷ enable testing of different classification methods on light curves. However, all these works are oriented towards obtaining a pure sample of SN Ia for cosmology, while a study on the combination of multiple selection effects and sources of uncertainty on the different science case of SN rate measurement (which requires having a complete sample of SNe, even if with lower purity) is still lacking. Our work acts as a complement of the previous analyses and aims at determining the impact of host galaxy association, photometric redshift and transients classification on the measurement of the SN Ia volumetric rate using a simulation of the first 5 years of LSST. We discuss all these effects one by one, to understand what should be improved to obtain an accurate evaluation of the SN Ia rate up to $z \sim 1$ with LSST.

3. The LSST DESC DC2 Universe

To build software pipelines ready to analyze the LSST data products, DESC produced a 300 deg^2 simulation of the first 5 years of survey as part of the Data Challenge 2 (DC2; [LSST Dark Energy Science Collaboration \(LSST DESC\) et al. 2021](#)). The simulation includes LSST-like images in all six optical bands *ugrizy*, processed with the LSST Science Pipelines⁸ (v.19.0.0). It is based on the *Outer Rim N*-body simulation ([Heitmann et al. 2019](#)), while the observing cadence is determined by the *min-ion_1016*⁹ strategy for the WFD survey with an average cadence of ~ 3 days in any filter. A smaller 1 deg^2 DDF with more frequent observations (up to one per day) is also included.

Simulated sources comprise stars, galaxies, variable stars and SN Ia (but no other SN types). SN Ia light curves are simulated starting from the rest-frame Spectral Energy Distribution (SED) of the SALT2-Extended model ([Guy et al. 2010](#); [Pierel et al. 2018](#)), which uses 5 parameters: redshift (z), time at peak brightness (t_0), amplitude (x_0), stretch (x_1), and color (c). The redshift distribution of SN Ia follows the volumetric rate $r_v(z) = 2.5 \times 10^{-5} (1+z)^{1.5} Mpc^{-3} yr^{-1}$ ([Dilday et al. 2008](#)) up to $z = 1.4$. SNe were assigned to galaxies with an occupation probability which scales with the galaxy mass. The SN position within the host traces the light in the galaxy sampled by the surface brightness profile of the disk and the bulge. SNe at $z > 1.0$ are not associated to galaxies while at lower redshift, 10% of SNe were randomly injected as host-less. Correlations between the SN type and the host galaxy properties are not included in the simulation.

The DC2 WFD region is also included in the LSST Data Preview 0 (DP0¹⁰), the first of three data previews serving as an early integration test of the LSST Science Pipelines and the Rubin Science Platform (RSP). A limited number of data rights holders has been granted access to the RSP, in order to start to familiarize with the Rubin Data Products¹¹ using a series of publicly available tutorials¹². DP0 has been released in three parts:

- DP0.1 (released on June 30, 2021) is the DESC processing of the data, focusing on static sky;
- DP0.2 (released on June 30, 2022) is the DC2 simulation reprocessed by the Rubin staff using version 23 of the LSST Science Pipelines and, and includes DIA data products;
- DP0.3 (released on August 2, 2023), LSST-like catalogues of solar system objects generated by the Solar System Science Collaboration¹³.

For more official references for DP0, see [O’Mullane \(2021\)](#), [Community Engagement Team & Operations Executive Team \(2022\)](#), and [O’Mullane et al. \(2023\)](#). All the galaxy catalogues used in this paper are extracted from DP0.2 and the codes used for the analysis have been successfully tested on the RSP, although the majority of the heavy tasks have been executed on DESC allocated space at NERSC¹⁴, which already contained all the necessary tables when this work started.

The sample of SN Ia analyzed in this paper comes from the work by [Sánchez et al. \(2022\)](#), which measured magnitude limits, detection efficiency, artifact contamination levels, and biases in the selection and photometry on a subset of $\sim 15 deg^2$ of the

⁶ lsst.org/scientists/keynumber

⁷ portal.nersc.gov/cfs/lsst/DESC_TD_PUBLIC/ELASTIC

⁸ pipelines.lsst.io

⁹ <https://docushare.lsst.org/docushare/dsweb/View/Collection-4604>

¹⁰ dp0-2.lsst.io

¹¹ Data Products Definitions Document (DPDD; ls.st/dpdd)

¹² github.com/rubin-dp0

¹³ dp0-3.lsst.io

¹⁴ National Energy Research Scientific Computing Center; nersc.gov

DC2 WFD region. To perform the analysis, they tested the LSST DIA pipeline on the selected region, using the first year to produce their own templates and the remaining 4 years for detection. The smaller region of sky and the shorter survey length (5 years instead of the planned 10) do not affect the final results.

There is a total of 5884 simulated SN Ia with $z \leq 1.0$ in the processed area. This number takes already into account all the objects not detectable because of gaps between the observing seasons or located in sky regions with subtraction artifacts from template overlapping issues. The number of SNe with at least one detection in one filter is 2186. Yet, for our analysis, we selected only sources detected in more than 5 distinct nights, in order to sample ~ 20 days on the light curve and have a more reliable classification. In case of multiple visits in the same night, we took the average magnitude for each detection. An example of the recovered SN Ia light curve at $z = 0.16$ is shown in Fig. 2. The condition on the minimum number of detections returned 600 SNe. The large drop of SNe after the cut on the minimum number of detections is mainly due to the sub-optimal observing cadence of the adopted survey strategy. The *minion_1016* strategy adopted by DC2 is indeed quite old, albeit it was most recent at the times of the simulation. Further analyses to improve the observing strategy are still ongoing, and the final cadence may improve the number of recovered SNe. Lochner et al. (2022) presented various metrics developed by DESC to analyze the cadences, highlighting the importance of low inter-night gaps in the redder filters for the selection of SNe. Possible improvements might also derive from a rolling cadence (Alves et al. 2023) or the higher coverage of the DDFs (Gris et al. 2023).

The final sample of SN Ia analyzed in this work consists then of 600 sources (hereafter, SN Ia sample) for which we know the true host galaxy and the true simulated redshift (z_{spec}). Throughout the paper, we treat them as a sample of candidate SNe of unknown type, ignoring all known parameters from the simulation and using only the recovered photometric information. We first associate each SN to the host galaxy with a procedure described in Sect. 4. Then we retrieve photometric redshifts for both the true (i.e., the simulation input) and the recovered host galaxies. Finally, we proceed with classification of light curves using the recovered redshifts as priors. Samples of SN Ia coming from each of these steps will produce a different distribution in redshift (see Sect. 5), thus affecting the SN Ia volumetric rate. The real case scenario consists of a sample of SNe classified as SN Ia using the photometric redshift of the associated host galaxy as a prior. Such a scenario includes a combination of all the effects analyzed in this work. We compute the SN Ia rate for different samples, alternatively analyzing each specific source of uncertainty in order to analyze the contribution of each effect separately and determine which one impacts most on the final uncertainty.

4. Host galaxy association

The association of SNe to the host galaxy is a key ingredient for the SN rate, but also for the SN photometric classification, as it provides an estimate of the SN redshift that can be used as prior in the classification (see Sect. 6). Indeed, as spectroscopic resources are limited, photometric redshifts of the host galaxies are an efficient way to obtain information on SN redshift. Moreover, the knowledge of the host galaxy and its properties enables the measurement of the SN rate as a function of the SFR, color, or the stellar mass of the galaxy (e.g., Sullivan et al. 2006; Botticella et al. 2017), and provides constraints on the SN progenitors (Wiseman et al. 2021).

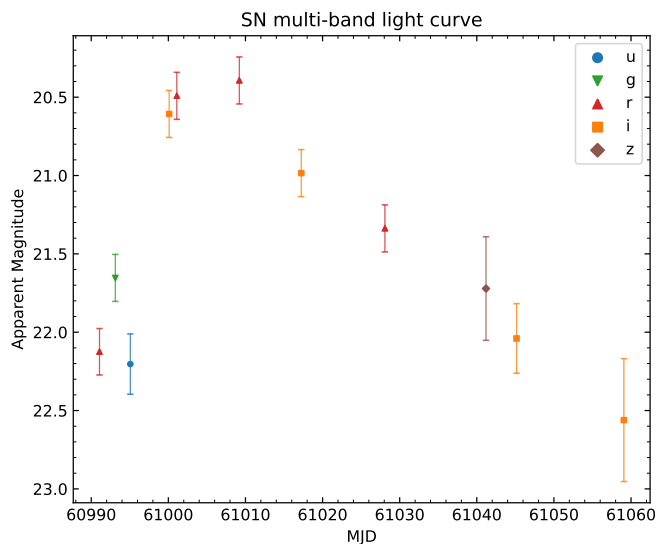


Fig. 2. Example multi-band light curve of a SN Ia with redshift $z = 0.16$. Different shapes and colors refer to different filters, as reported in the legend.

We associate transients to galaxies using only information about the galaxy light profile and the angular separation from SNe. More complicated approaches could include any correlations between the SN type and the host galaxy properties, which are not included in this simulation. Recent reviews of host association algorithms, also using postage stamps of a field surrounding the transient, are reported in Gagliano et al. (2021) and Förster et al. (2022), the latter implementing a novel deep learning approach. We developed our own code which adapts the calculation of the Directional Light Radius (DLR; Gupta et al. 2016) to the Rubin Data Products and produces cutouts through the RSP to evaluate the results. The DLR is the elliptical radius of a galaxy in the direction of the SN in units of arcseconds. This metric takes also the extension and the orientation of the galaxies into account, and produces more reliable physical associations than using the plain angular separation. The DLR method, using only catalogue information, is fast and scalable to all kinds of extragalactic transients, as it makes no assumptions on its nature. Our code is publicly available and ready to work with Rubin Data Products on the RSP¹⁵.

For each SN, we select host galaxy candidates in a region of $30''$ radius around the SN coordinates from the catalogue of static sources detected on stacked images (i.e., the LSST Object table). Such a radius is typically used in literature and is big enough to include the hosts of extragalactic transients. The full catalogue resulting from the query includes 277 852 galaxies (hereafter, *candidates*). Such a sample is also used in Sect. 5 to assess the quality of photometric redshifts, as it is big enough to include all typical DP0 galaxies.

We assume the isophotes of the galaxy are self-similar ellipses and get the Stokes parameters Q and U from the adaptive second moments of source intensity I_{xx} , I_{yy} , I_{xy} :

$$Q = I_{xx} - I_{yy} \quad (2)$$

$$U = I_{xy} \quad (3)$$

¹⁵ github.com/vpetrecca/Rubin-DP0-host-association

The position angle (east of north) ϕ and the axis ratio A/B of the galaxy are then

$$\phi = \frac{1}{2} \arctan\left(\frac{U}{Q}\right) \quad (4)$$

$$A/B = \frac{1 + k + 2\sqrt{k}}{1 - k} \quad (5)$$

where k is derived from the Stokes parameters as

$$k \equiv Q^2 + U^2 = \left(\frac{A - B}{A + B}\right)^2 \quad (6)$$

We then measure the position angle α of the SN relative to the candidate host galaxy and we combine it with the angle ϕ to get the angle θ that the SN makes with the semi-major axis of the galaxy. Using the equation of an ellipse in polar coordinates with the origin at the center of the galaxy, we get the elliptical radius of a galaxy in the direction θ , which is the definition of the DLR:

$$r(\theta) = \frac{A}{\sqrt{(A/B \sin \theta)^2 + (\cos \theta)^2}} \equiv DLR \quad (7)$$

As an estimate of the semi-major axis A , we use a value of 2.5 times the Kron radius, that includes $> 96\%$ of the total flux of a galaxy (Kron 1980). Finally, we define a dimensionless quantity by normalizing the angular separation d_{sep} between the SN and the candidate host by DLR:

$$d_{DLR} \equiv \frac{d_{sep}}{DLR} = \frac{d_{sep}}{A} C \quad (8)$$

where C is the denominator of Eq. 7. In this way, we define a quantity which weights the SN radial distance by taking into account both the extension (the Kron radius, A) and the orientation (the C parameter) of the galaxy.

For each SN, we rank all candidate galaxies by increasing d_{DLR} and pick the one with the minimum d_{DLR} as the best host. If minimum $d_{DLR} > 4$, we define the SN as host-less (SNe originally simulated as host-less in DC2 had been removed from the sample). As a further cut, we rejected candidate galaxies with i -band magnitudes $mag_i \geq 24.5$ and with bad-quality fitting flags. These cuts reduce misassociations due to badly estimated galaxy parameters, mostly happening for low S/N sources. By looking at the distributions of candidates parameters, we also reject galaxies with Kron radii $\geq 7.5''$ or Kron radii $\leq 1.4''$ to reduce misassociations due to catastrophic estimates of the galaxy extension (see Fig. 3). All these cuts have an impact of only 1% on the true host galaxy sample. We point out that the DLR method is strongly dependent on the quality of galaxy fitting. The Kron radii used in this work are computed using version 23 of the LSST Science Pipelines. Newer versions may improve the quality of galaxy parameters and require different cuts.

By comparing the results of our algorithm with the simulation input, we find that 89% of SNe are correctly associated to the true host. Among the misassociations, 8 (i.e., $\sim 1\%$ of the total, 12% of the wrong) are recovered as host-less, 35 (55% of the wrong cases) are faint galaxies with $mag_i > 22$. The remaining 33% is a result of projection issues (i.e., a bright galaxy along the line of sight of a SN actually injected into a faint host), or two similar galaxies in terms of morphology and angular separation from the SN, producing a similar d_{DLR} . Cutouts with examples of associations are reported in Fig. 4 for a correct case and two misassociations from the cases described above.

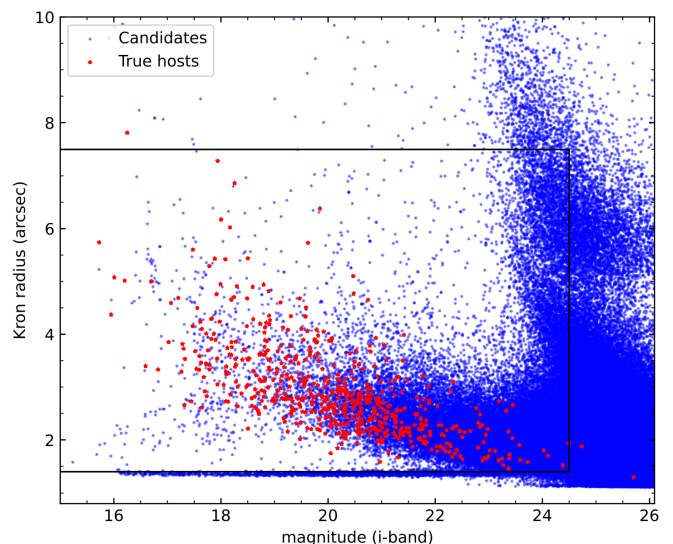


Fig. 3. Kron radii and i -band magnitudes for the entire sample of host candidate (blue dots) and true (red stars) SN host galaxies. The black square determines the region actually used for the host association, avoiding faint galaxies and catastrophic estimates of the Kron radii.

Misassociations may also alter the distribution of the parent galaxy properties, affecting the final measurement of the SN rate. Figure 5 shows how the magnitude distribution of the SN hosts changes moving from the true to the associated host galaxies (hereafter denoted with “_best”). While there is an overall agreement for bright sources, it is worth noticing an excess of galaxies with $mag_i > 22.5$ for those associated with the DLR method. This will also have an effect on the accuracy of photometric redshifts, which tends to be lower with fainter sources as explained in Sect. 5.

The association using only the minimum angular separation has a lower efficiency of 81%. This highlights the importance of using more complex approaches as the DLR to associate transients to the host galaxies. Even better results could be obtained by considering correlations between the SN type and the galaxy properties, which are not included in this simulation.

5. Photometric redshifts

We cross-matched both the catalogues of true and associated host galaxies with a catalogue of photometric redshifts (z_{phot}) for DC2 galaxies produced by Schmidt et al. (2020) with the BPZPipe code¹⁶, which employs a training set complete up to $mag_i \leq 25.0$. We used the weighted mean value of the posterior probability density function (PDF) for each galaxy as a point estimate of the photometric redshift.

To assess their quality, we used the sub-sample of all candidates host galaxies with $mag_i \leq 25$ and $z_{spec} \leq 1.0$, composed of 43161 objects. By following the approach of Graham et al. (2018), we define a z_{phot} error as $\Delta z = (z_{spec} - z_{phot}) / (1 + z_{phot})$, where z_{spec} is the true simulated redshift. The robust standard deviation of the z_{phot} error is evaluated in the interquartile range (IQR) containing 50% of the catalogue galaxies. The value is then divided by 1.349 to convert it to the standard deviation of a Gaussian distribution (σ_{IQR}). This returns a value of $\sigma_{IQR} = 0.05$ on the catalogue of all galaxies, and $\sigma_{IQR} = 0.03$ on the true host galaxies of the SN Ia. The fraction of outliers (i.e., with

¹⁶ github.com/LSSTDESC/BPZpipe

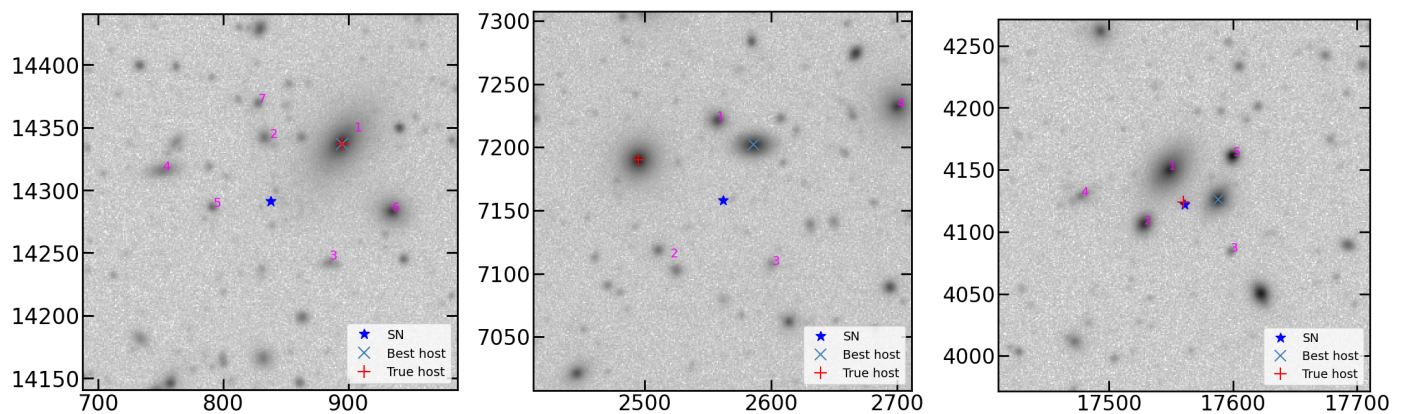


Fig. 4. Cutouts around SNe (blue star) extracted with the RSP. The magenta numbers identify possible host galaxies (ranked according to the lowest d_{DLR}), the blue x represents the best host candidate (the zeroth galaxy in the ranked list), while the red cross + is the true host galaxy of the simulation. From left to right there are i) an example of correctly associated SN, and two possible misassociation cases: ii) very similar galaxies in terms of morphology and angular separation from the SN; iii) true host galaxy extremely faint and not among the possible list of candidates.

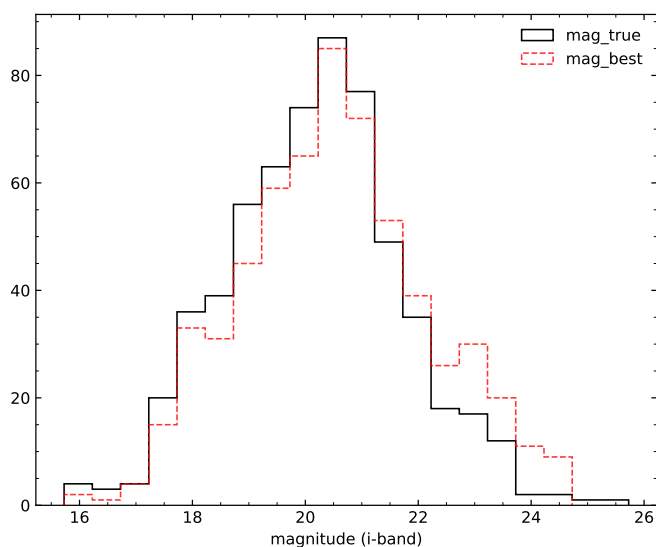


Fig. 5. Distribution of i-band magnitude for the SN Ia host candidates. The black solid line is the magnitude of the true host galaxy (i.e., simulation input), while the red dotted line denotes the hosts associated with the DLR method.

$\Delta z > 3\sigma_{IQR}$ is 7% for the catalogue of all galaxy candidates and 5% for the SN Ia hosts. The comparison between the simulated and photometric redshift for both the sample of all candidate hosts and the true hosts is shown in Fig. 6, where the better agreement for the true hosts is clearly evident as they are generally massive and brighter (see Fig. 3). The horizontal line at the bottom of the plot identifies catastrophic outliers $z_{phot} \leq 10^{-5}$, and 15 of them refer to true SN Ia hosts. Through all this work, we will adopt a fixed value of uncertainty of 0.05 on each photometric redshift estimate, as coming from the analysis of σ_{IQR} on the galaxy catalogue. The value is also consistent with analysis of the median FWHM of the peak in the z_{phot} PDFs.

Figure 7 shows the combined impact of photometric redshift and host galaxy association on the retrieved SN sample redshift distribution. As expected, the redshift distribution of the SN hosts appears wider when using the photometric redshift of the associate host (z_{phot_best}). This is especially true for faint galaxies whose uncertainty on photometric redshift is higher. We

notice a peak at $z_{phot} \sim 0$ due to catastrophic outliers or SNe wrongly associated to nearby galaxies, and a peak at $z_{phot} \sim 0.45$ mainly due to the known degeneracy between the Lyman break of galaxies at higher redshift and the Balmer break of galaxies at lower redshift (Massarotti et al. 2001; Salvato et al. 2019). These peaks, together with an excess of sources at higher redshifts, result in a decrease of SNe in all the other redshift bins.

In Sect. 7 we will quantitatively discuss the effect of the changing distribution on the volumetric rate by considering redshift bins of width 0.05 (which is the nominal error on photometric redshifts). The analysis is restricted to the redshift range $0.1 \leq z \leq 0.7$ to avoid a catastrophic drop of simulated SNe at the edges of the distribution. As shown in Fig. 7, we expect a loss of SNe in all the redshift bins with an excess at $z_{phot} \sim 0.45$. We also point out that, in principle, all the effects of bin migration arising from this work could be taken into account with a Monte Carlo analysis leading to correction coefficients (see e.g., Lasker 2020). However, estimating the proper corrections taking into account all sources of uncertainty (including those related to the detection) would require producing more DP0-like simulations. The present work focuses only on what is provided in DP0.2, as a single realisation of the Universe processed with the LSST science pipelines. The production of more complete simulations is under investigation for future works.

6. Classification

For large surveys like LSST, the photometric classification of transients is an essential task. Although the brokers will instantly process the nightly alert streams¹⁷, this will mainly serve as a pre-classification to enable follow up of specific sources of interest with other facilities. More thorough analysis may require a posteriori classification using all the available information.

In this section, we present the results of the classification with three different approaches, based on light curves of the SN Ia sample. The first two methods involve template fitting and are part of the publicly available SuperNova ANALYSIS software package (SNANA¹⁸; Kessler et al. 2009), while the last one uses a recurrent neural network (RNN) trained on light curves. For all the methods, we obtain a classification: i) using only light

¹⁷ lsst.org/scientists/alert-brokers

¹⁸ <https://github.com/RickKessler/SNANA>

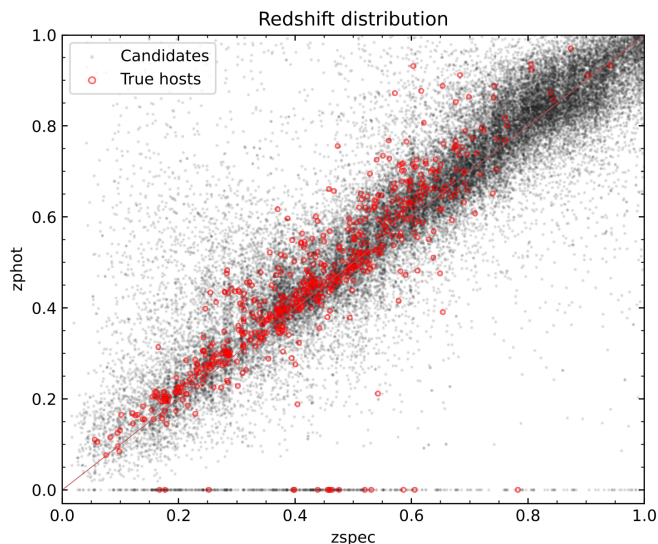


Fig. 6. Distribution of the true simulated redshift (z_{spec}) and photometric redshifts (z_{phot}) for a sample of galaxies with $mag_i \leq 25$. Black dots are for all host candidates, red open circles are the true SN Ia hosts.

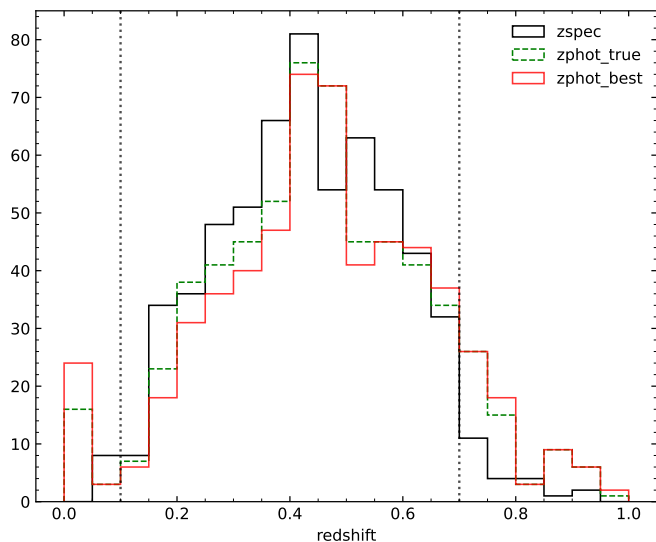


Fig. 7. Distribution of redshift for the SN Ia host candidates. The black one uses the true simulated redshift (z_{spec}), the green dashed line represents the photometric redshift of the true host galaxy ($z_{\text{phot_true}}$), while the red continuous distribution refers to the photometric redshift of the associated host galaxy ($z_{\text{phot_best}}$). The two vertical lines define the range where we evaluate the volumetric rate and the plot is cut to $z = 1.0$ for visual clarity.

curves, ii) providing the photometric redshift of the associated host galaxy as a prior (if available¹⁹), iii) providing the true simulated redshift as a prior, which is the case when we have the spectroscopic redshift of the true host galaxy from other surveys.

The final results of the classification, using all the methods, are summarized in Table 1. Although our classification models have been trained on multiple classes, the presence of SN Ia only in the DC2 simulation does not allow us to measure the actual effect of contamination from other transients (especially from SN

¹⁹ SN Ia identified as host-less or having catastrophic photometric redshifts (i.e., $z_{\text{phot}} \leq 10^{-5}$) are classified with a flat prior on redshift.

Ib/c). The mis-classification effect will then only be a reduction of the total number of SN Ia from the original sample. We refer to upcoming works analyzing the ELASTiCC light curves for a deep overview of photometric classification.

6.1. PSNID

The Photometric SuperNova IDentification (PSNID; Sako et al. 2011) is a template fitting algorithm which calculates the reduced χ^2 against a grid of SN Ia light curves models and core-collapse SN templates in order to identify the best-matching SN type. It has been firstly used for prioritizing spectroscopic follow-up observations for the SDSS-II SN Survey (Sako et al. 2008), and it has been also tested with SNANA simulations from the Supernova Photometric Classification Challenge (Kessler et al. 2010).

The version we used is integrated in SNANA and computes also Bayesian probabilities for different SN types. More into detail, the Bayesian evidence E for each SN type is calculated by marginalizing the product of the likelihood function and prior probabilities over the model parameter space:

$$E_{\text{type}} = \sum_{\text{template}} \int_{\text{pars. range}} P(z) e^{-\chi^2/2} dz dA_V dT_{\text{max}} d\mu \quad (9)$$

Fitting parameters are redshift z , with probability distribution $P(z)$, extinction A_V , time of maximum T_{max} and distance modulus μ . In this work, priors in A_V , T_{max} and μ are flat, while for redshift we tested both a flat prior with $P(z) = 1$, and a Gaussian prior by providing the mean and sigma as described in Sect. 5 when using the photometric redshifts, and a sigma of 0.0001 when using the spectroscopic prior. For the SN Ia light curves we used the SALT2-Extended model (Pierel et al. 2018), the same that had been used in the simulation, while templates for SNe core-collapse come from Vincenzi et al. (2019). SN template light curves are K-corrected using tables produced for LSST by DESC.

The Bayesian probability for each SN type is then defined as

$$P_{\text{type}} = \frac{E_{\text{type}}}{E_{Ia} + E_{Ib/c} + E_{II}} \quad (10)$$

where

$$P_{Ia} + P_{Ib/c} + P_{II} = 1. \quad (11)$$

With both Bayesian probability and χ^2 available, there are many ways of selecting a sample of SN Ia. PSNID comes with a default criterion which takes both of them into account and defines the SN as of "unknown" type if the difference between the χ^2 of two SN types is smaller than a certain threshold. However, as discussed in Kuznetsova & Connolly (2007), the minimum χ^2 alone is not always a good indicator of the best SN type. This become even worse when small photometric errors lead to unreasonably high values of χ^2 . While the issue is often mitigated by artificially increasing the errors on light curves, we preferred to rely only on the Bayesian probability and selected all SNe with $P_{Ia} > 0.5$. With this conservative approach, we maximize the completeness of the sample, which is very important for the evaluation of the SN rate. Figure 8 shows an example of template fitting resulting in a SN Ia according to the Bayesian probability, but of unknown type when using the χ^2 .

The fractions of SNe correctly classified as SN Ia are very high when the redshift prior is used (95% with the associated

zphot and 99% with the true simulated redshift). However, without a prior on redshift, only 44% of SNe are correctly classified, and the resulting redshift distribution is peaked towards lower values. This occurs because of a degeneracy between extinction and redshift in the light curves reddening and it shows the importance of using priors, when available.

6.2. SALT2 fitting

Another approach often used in SN Ia cosmology consists of fitting a selected model to the light curves and taking only those candidates providing good fits (e.g., [Sánchez et al. 2022](#); [Mitra et al. 2023](#)). The resulting sample will have high purity, which is essential for cosmological analysis, but the procedure only allows to select sources conforming to the predefined model.

As our sample contains only SN Ia, we tested this methods using the software *snlc_fit.exe* distributed by SNANA and assuming again the SALT2-Extended model. The best fit is determined through a minimization procedure based on CERNLIB’s MINUIT program²⁰ and two iterations on each light curve. The fitting requirements are very similar to those adopted in [Sánchez et al. \(2022\)](#) on the same dataset:

- stretch parameter $|x_1| < 3$;
- color parameter $|c| < 0.3$;
- fit probability (P_{fit}) computed from χ^2 and number of degrees of freedom satisfying $P_{fit} > 0.05$.

Similarly to what we did with PSNID, we tested the SALT2 fit both with a Gaussian prior on redshift and with no redshift prior.

The fitting procedure results in a selection efficiency of 75% when the photometric redshift of the associated galaxy is used as a prior, and 69% with no redshift information. The success fraction for the no-zphot prior scenario when using SALT2 fitting is higher than that of PSNID. The main reason is that PSNID is doing a more complicated classification between different classes, while here we are just fitting a single model to all our sources.

6.3. SuperNNova

Recent advantages in deep neural networks make them extremely promising to photometrically classify variable sources for large surveys like LSST. Indeed, they can be trained on both simulated and archival data, enabling a fast multi-class analysis not limited either by costly feature extraction or by template matching biases. SuperNNova²¹ (SNN; [Möller & de Boissière 2020](#)) is an open-source framework requiring only photometric time-series as input, with additional information (e.g., host galaxy redshift) that can be provided to improve performances. SNN includes different classification methods, as long short-term memory (LSTM; [Hochreiter & Schmidhuber 1997](#)) recurrent neural networks (RNNs) and two Bayesian neural networks (BNN).

As with the previous approaches, we tested SNN on our SN Ia sample both with and without redshift information using the default configuration RNN. We trained our models using a sample of synthetic light curves of all SN type with LSST like photometric performances from ELASTiCC. The simulation also includes spectroscopic and photometric host galaxy redshifts for ~ 5 million objects, thus allowing to build training sample with different redshift priors. We trained 3 different models for a binary SN Ia vs non-Ia classification: i) light curves only, ii) with

host galaxy photometric redshift, iii) with spectroscopic redshift. The SNN output is a probability of being SN Ia, P_{Ia} , for each SN event. We considered as correctly classified all SN with $P_{Ia} > 0.5$. This resulted in 96% or 97% accuracy when the photometric or spectroscopic redshift information is used (compatible with PSNID). However, without redshift prior, only 80% of SNe is correctly classified as SN Ia.

The lower efficiencies for all the methods in absence of redshift information show how fundamental it is to have reliable estimates of photometric redshifts and a good host association procedure. This is especially true if the number of detections and their distribution around the light curve peak is not sampled enough to enable a proper classification (see e.g., [Alves et al. 2022](#)).

Method	no z prior	zphot_best prior	zspec prior
PSNID	44%	95%	99%
Salt2 fit	69%	75%	80%
SuperNNova	80%	96%	97%

Table 1. Fraction of correctly classified SNe from the SN Ia sample using different methods.

7. SN Ia Rate

The measurement of the SN rate requires accurate information on the survey strategy and design, both for what concerns the detection efficiency and the observing cadence. The former is usually determined with simulations and injection of point-like sources onto images, exploring a wide range of magnitudes and positions on sky ([Cappellaro et al. 2015](#)). The impact of the latter is traditionally measured with the *control time* ([Zwicky 1942](#)), defined as the interval of time during which a SN occurring at a given redshift is expected to remain above the detection limit of the image.

However, the DC2 observing strategy is not the definitive version that will be adopted for LSST. Moreover, the main aim of this work is the analysis of the impact on the rate of sources of uncertainties that are not directly related to the survey strategy. For this reasons, we adopted a simplistic approach consisting in evaluating a single *recovery efficiency* term, which takes into account both control time and detection efficiency, from the simulated rate. We refer to other works for a thorough analysis of detection efficiency and magnitude limits on DC2 simulation ([Sánchez et al. 2022](#)) and the impact of different observing cadence on the classification of SNe ([Alves et al. 2022](#)).

We considered the SN Ia sample in the range $0.1 \leq z_{spec} \leq 0.7$ (as explained in Sect. 5), and divided it in redshift bins of width 0.05, which is the typical error of a photometric redshift measurement. The selected range of redshift contains 570 of the 600 SN Ia in the SN Ia sample. We define the *recovery efficiency* as the ratio of the number of detected sources in the SN Ia sample to the total number of simulated SN Ia in each redshift bin over an observing window of $T = 3.5$ years, which is the effective observing time removing gaps between seasons. The distributions with the number of simulated and detected SN Ia in the redshift bins is showed in Fig. 9, while the ratios leading to the *recovery efficiency* ϵ are reported in Table 2.

Depending on the adopted estimate of redshift, the distribution of SNe is different, as showed in Fig. 7. The total number of recovered SN Ia when looking at photo-z is lower than those in the simulated sample because of sources being assigned

²⁰ root.cern.ch/doc/master/classTMinuit.html

²¹ github.com/supernnova/SupernNova

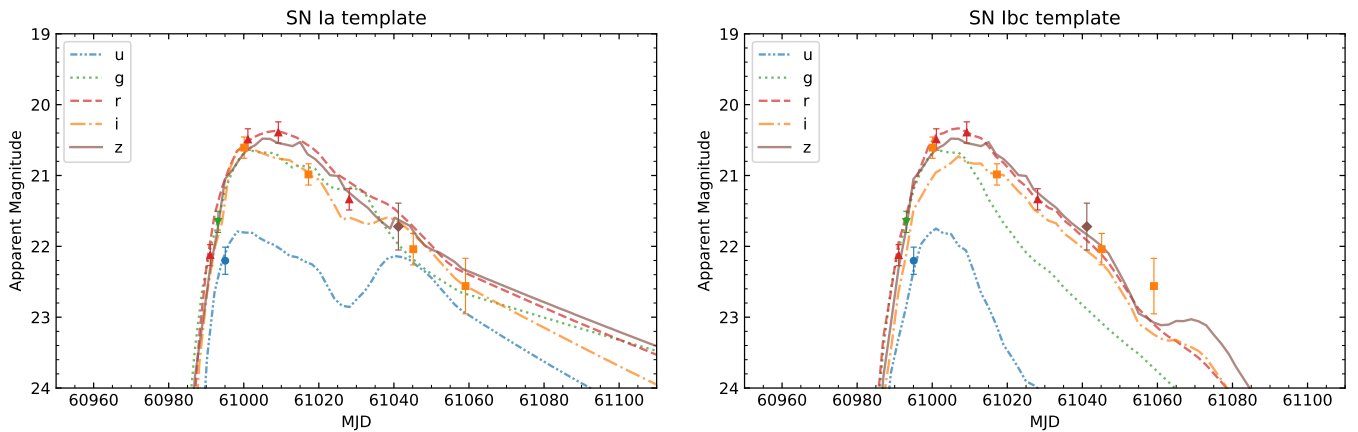


Fig. 8. Example of template fitting with PSNID for a SN Ia and a SN Ib/c model on the same light curve. Different colors and lines refer to different photometric bands. Left panel shows the fitting with the best Ia template, while the right panel shows the best-fitting SN Ib/c template. Although both fits seem reasonable, not allowing a straightforward classification, the type Ia has a Bayesian probability $P_{Ia} = 1.0$ with the redshift prior.

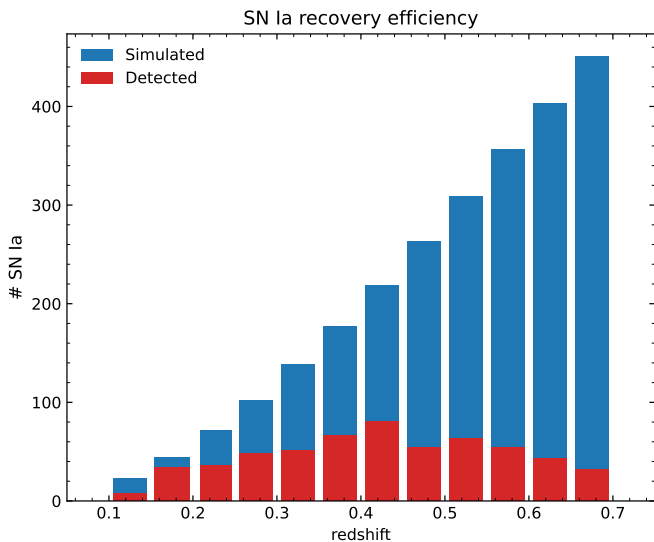


Fig. 9. Numbers of SN Ia simulated (blue) and detected (red, the SN Ia sample) in the redshift bins used for the measurement of the rate.

a redshift outside the selected range. Moreover, additional SN Ia are lost because of mis-classifications and the absence of non-Ia contaminants. In this section, we evaluate (separately) the uncertainty contribution of photometric redshifts, host galaxy association and photometric classification on the measurement of the SN Ia rate. As a reference classification tool, we use PSNID adopting the `zphot_best` prior of the associated galaxy. The reasons for this choice are the flexibility of the algorithm in dealing with different SN types, the possibility to customize the output by defining an "unknown" class, and the fast execution (intrinsically parallelizable) without requiring to build new training sets. The classification accuracy of the other multi-class algorithm (SuperNNova) is similar, thus the choice of the classification method does not affect the final result.

The samples used in our analysis are the following:

- **`zphot_true`**: SN Ia sample adopting the photometric redshift of the true host galaxy instead of the true simulated redshift (this allows to test the effect of photometric redshift);

Simulated	Detected	Bin	ϵ
23	8	$0.10 \leq z < 0.15$	34.8%
44	34	$0.15 \leq z < 0.20$	77.3%
71	36	$0.20 \leq z < 0.25$	50.1%
102	48	$0.25 \leq z < 0.30$	47.1%
138	51	$0.30 \leq z < 0.35$	37.0%
177	66	$0.35 \leq z < 0.40$	37.3%
219	81	$0.40 \leq z < 0.45$	37.1%
263	54	$0.45 \leq z < 0.50$	20.6%
309	63	$0.50 \leq z < 0.55$	20.4%
356	54	$0.55 \leq z < 0.60$	15.2%
403	43	$0.60 \leq z < 0.65$	10.1%
451	32	$0.65 \leq z \leq 0.70$	7.1%

Table 2. SN Ia recovery efficiency ϵ in different redshift bins.

- **`zphot_best`**: SN Ia sample adopting the photometric redshift of the associated host galaxy (effect of photometric redshift + host galaxy association);
- **`psnid_zphot_best`**: sample of SNe correctly classified as SN Ia adopting the photometric redshift of the associated host galaxy as a prior (effect of photometric redshift + host galaxy association + classification uncertainties).

A first measurement of the contribution of the different effects comes from the lost fraction of SNe for the various samples Δ_{sample} , providing an indication of the number of SN Ia lost because of wrong photometric redshift, host association and classification. We define it in each redshift bin as:

$$\Delta_{sample} = (N_{detected} - N_{recovered})/N_{detected}, \quad (12)$$

where $N_{detected}$ refers to the original SN Ia sample (not affected by the uncertainties analyzed in this work) and $N_{recovered}$ is the number of SN Ia in each one of the samples defined above. The resulting values as a function of redshift are shown in Fig. 10 with different colors for the different subsets. As already noticed by looking at the redshift distribution in Fig. 7, there is an overall depletion of SNe with the exception of the bins at $z \sim 0.45$ and $z > 0.6$. The `sample_psnid_zphot_best`, which include all the effects together, has an average lost fraction of 17%. However, photometric redshift alone, measured with the

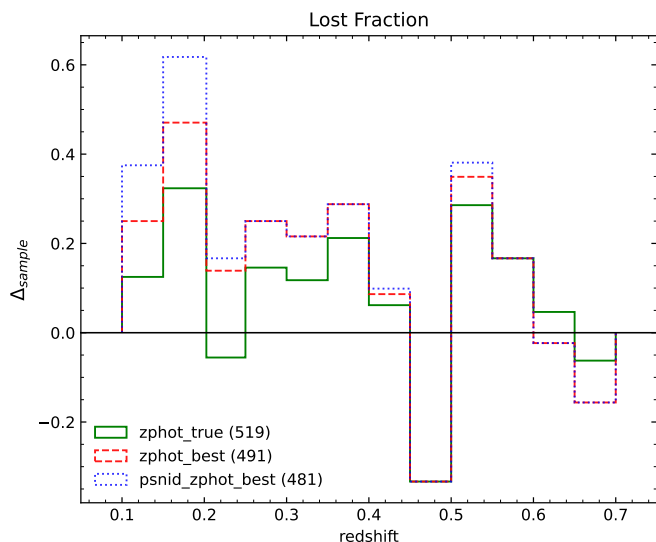


Fig. 10. Lost fraction of SNe in each redshift bin for the different samples, highlighting the impact of photometric redshift ($z_{\text{phot_true}}$), host galaxy association ($z_{\text{phot_best}}$), and classification ($psnid_zphot_best$). The numbers in parenthesis refer to the total number of SNe in each subset for the selected redshift range. Negative values of Δ_{sample} denote an increase of sources in that redshift bin (see Eq. 12).

$sample_zphot_true$, has an impact of 10% and results to be the major source of uncertainty (also affecting classification when used as prior). It is also worth noticing how the different effects depend on redshift: at $z > 0.4$ most of the mismatch comes from the error on the photometric redshift, while lower redshifts are more affected by wrong host galaxy associations and wrong photometric classification.

We now want to test what is the effect of the different biases on the derived SN rates. To this aim, we compute the SN Ia volumetric rate for each sample as:

$$r_{SN Ia}(z) = \frac{(1+z) N_{SN}(z)}{V(z) T \epsilon(z)}, \quad (13)$$

where $N_{SN}(z)$ is the number of SNe in each redshift bin for the selected sample, T is the observing window, $(1+z)$ corrects for time dilation, $\epsilon(z)$ is the SN Ia recovery efficiency defined in Table 2, and $V(z)$ is the comoving volume for the given redshift bin:

$$V(z) = \frac{4\pi}{3} \frac{\Theta}{41253} \left[\frac{c}{H_0} \int_{z_1}^{z_2} \frac{dz'}{\sqrt{\Omega_M(1+z')^3 + \Omega_\Lambda}} \right]^3 \text{Mpc}^3. \quad (14)$$

In the previous equation, Θ is the search area of 15 deg^2 , z is the mid-point of the redshift interval $[z_1, z_2]$, and we assumed a flat Λ CDM universe with $H_0 = 70$ and $\Omega_M = 0.3$.

The resulting SN Ia rates for the different samples are shown in Fig. 11, along with power-law fits with the same functional form of the simulated rate from Dilday et al. (2008):

$$r_v(z) = \alpha \times 10^{-5} (1+z)^\beta \text{Mpc}^{-3} \text{yr}^{-1}. \quad (15)$$

The fit results are summarized in Table 3. The differences between the fit parameters and the input rate ($\alpha = 2.5$ and $\beta = 1.5$) show that the uncertainties not only reduce the number of SN Ia in each redshift bin, but also change the evolutionary trend of the recovered rate. The combination of the two effects hampers

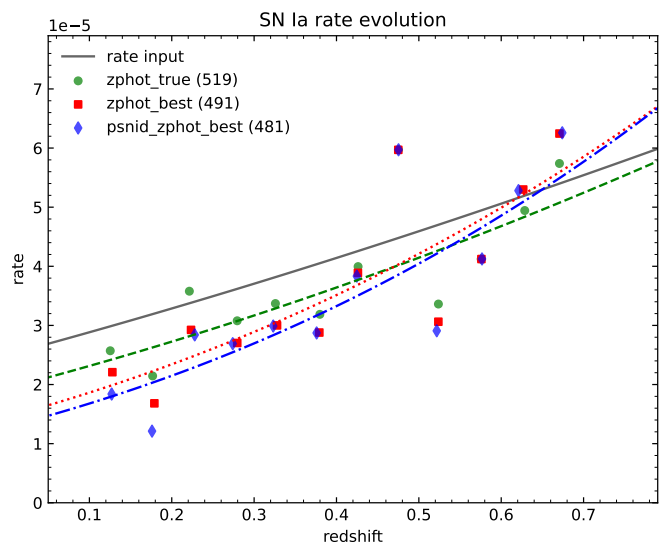


Fig. 11. SN Ia rate for the different samples, as in Fig. 10. Continuous lines are power-law fits of the rate points. Error bars due to statistical uncertainty are omitted for visual clarity.

the use of the volumetric rate to discriminate between SN Ia progenitor models, unless the impact of these sources of uncertainty can be reduced.

To quantitatively address the problem, we focused on the $sample_psnid_zphot_best$, which represents a real case scenario combining all the uncertainties (i.e., a study of SN Ia rate with photometric data only). Figure 12 shows the recovered rate along with predictions from the progenitor models described in Sect. 1 (where the k_{Ia} factor in Eq. 1 has been fixed to $0.8 \times 10^{-3} M_\odot^{-1}$ for all scenarios). Error bars on the blue point are due to statistical uncertainties scaled to 10 years over the simulated $\sim 15 \text{ deg}^2$ (even though we expect higher statistics with the real survey, with statistical errors reduced by more than one order of magnitude). The grey points represent rate measurement from the literature, as shown in Fig. 1. It is clearly evident how LSST will reduce the scatter between the rate estimates obtained comparing multiple surveys up to $z \sim 1.0$. However, biases introduced by other sources of uncertainty, such as those analyzed in this work, should still be reduced to attain optimal results. Despite Fig. 1 showed that in the intermediate redshift range probed by LSST different progenitor models have similar outcomes, the combination of LSST and higher redshift surveys (e.g., the Nancy Grace Roman Space Telescope; Rose et al. 2021; Wang et al. 2023) could indeed allow to distinguish between different scenarios. Moreover, Greggio & Cappellaro (2019) show that the SN Ia rate as a function of host galaxy colors or specific SFR is even more efficient in separating the predictions of different models, once all the uncertainties have been reduced.

Sample	α	β	α_{err}	β_{err}
zphot_true	1.9	1.9	0.3	0.4
zphot_best	1.4	2.6	0.3	0.4
psnid_zphot_best	1.3	2.8	0.3	0.5

Table 3. Fit coefficients for all the samples. The input rate has $\alpha = 2.5$ and $\beta = 1.5$.

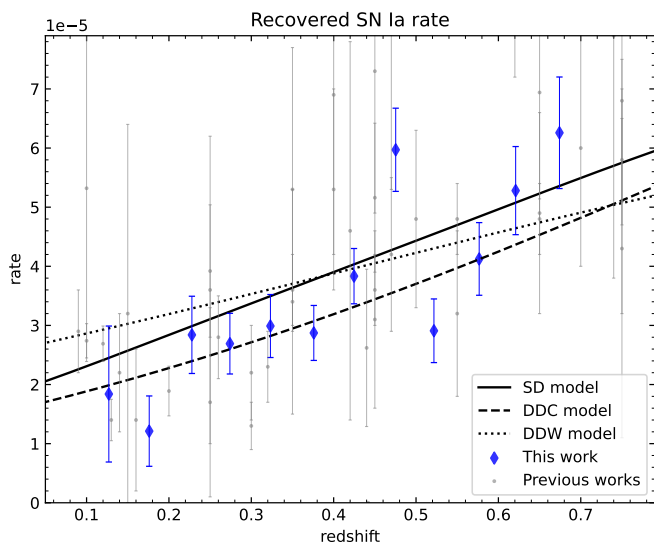


Fig. 12. The recovered SN Ia rate for the *sample_psnid_zphot_best* (the real observing case) with rate predictions of progenitor models from Greggio (2005). Error bars on the blue points are due to statistical uncertainties scaled to 10 years over the simulated $\sim 15 \text{ deg}^2$ DC2 universe (even though we expect higher statistics with the real survey). The grey points are the literature measurements shown in Fig. 1.

8. Summary and conclusions

The LSST is expected to increase the number of detected SN Ia by a factor of 100 compared to samples from previous surveys (Jones et al. 2019). This will dramatically reduce statistical uncertainties on the SN Ia rate measurement, possibly allowing us to put constraints on the SN Ia progenitors by comparing the observed rate with predictions from theoretical models. However the actual impact of all the possible sources of uncertainty on the measurement of the rate deserves further analysis. While many observational biases in the selection of a good sample of SN Ia for cosmology have already been inspected in other works, here we studied the uncertainties due to estimate of photometric redshift, host galaxy association and classification on the measurement of the SN Ia rate using simulated LSST images.

Data come from Sánchez et al. (2022), who executed DIA on a subset of $\sim 15 \text{ deg}^2$ of the DC2 simulation. There are a total of 5884 simulated SNe with $z \leq 1.0$, 2186 of them detected on difference images. We selected only sources with more than 5 distinct detections in order to have a sufficiently sampled light curve for the transient classification. The analyzed SN Ia sample consists than of only 600 sources, an order of magnitude lower than the number of simulated SN Ia. The large loss of sources is mainly due to the sub-optimal observing cadence of the simulated WFD region and testifies the need of heavily cadenced observations on smaller region of the sky for significant statistical studies. Indeed, the definition of the best cadence is still an open issue and there are many works using simulations to provide quantitative metrics (e.g., Lochner et al. 2022).

We associate each SN Ia to the host galaxy using the DLR. Our algorithm has an association accuracy of 89% using only morphological information extracted from a single band deep coadd image. Among the misassociation, 12% is recovered as host-less, 55% is associated to a faint galaxy with $\text{mag}_i > 22$, and the remaining 33% is a combination of projection issues or two similar and close galaxies producing a similar d_{DLR} . The host association could be further improved with a better estimate of

the photometric parameters for faint galaxies and by considering also the correlation between the SN type and the host galaxy properties (not included in the simulation).

We recovered estimates of the SN photometric redshifts from both the true and the associated host galaxy. The quality of the photometric redshift has been studied with a sample of galaxies with $\text{mag}_i \leq 25$ and $z_{\text{spec}} \leq 1.0$. The analysis returned a robust standard deviation of $\sigma_{IQR} = 0.05$ and the fraction of outlier is 7%. The combined impact of photometric redshift and host galaxy association results in a broadening of the SN Ia distribution in redshift. We found an excess of associated host galaxies with $\text{mag}_i > 22.5$, along with a peak at $z_{\text{phot}} \sim 0$ (due to catastrophic outliers or SNe wrongly associated to nearby galaxies), and a peak at $z_{\text{phot}} \sim 0.45$ (mainly due to the known degeneracy between the Lyman break of galaxies at higher redshift and the Balmer break of galaxies at lower redshift).

Light curves have been classified with different methods, involving both template fitting techniques (PSNID and SALT2 model fit by SMANA) and recurrent neural networks (SuperNNova). All the algorithms have been executed with and without prior on redshift, proving the improvement of classification accuracy (up to 96%) when redshift information is included. In our subsequent analysis of the SN Ia rate, we used the results of PSNID with photometric redshift of the associated host galaxy as a prior. The only effect of mis-classified SNe is a decrease in the number of sources, because no other SN type is included in the simulation. Real life scenario would also include contamination from other transients, especially from SNe of type Ib/c.

The SN Ia rate was measured on different samples to evaluate separately the impact of uncertainties due to photometric redshift, host galaxy association and classification. For each sample, we divided SN Ia in redshift bins of width 0.05 (which is the typical error of a photometric redshift estimate) in the range $0.1 \leq z_{\text{spec}} \leq 0.7$ and normalized the rate to the input model of the DC2 simulation. The different distribution in redshift of the various samples led to an average 17% mismatch in the recovered fraction of SN Ia with respect to the original SN Ia sample. As 10% of it is due to photometric redshifts alone (which also affect the classification), having good photometric redshift estimates results to be the major issue in the measurement of the SN Ia rate. The uncertainties not only change the number of SN Ia in each redshift bin, but also change the evolutionary trend of the recovered rate, hampering the discrimination between different progenitor models.

Despite our estimate of the uncertainties might be reduced in the near future (e.g., using better algorithms, improving the measurement procedure, including additional information, etc.), we showed they are still relevant and have a significant impact on the rate measurement. Their reduction will be fundamental for precision SN Ia science, both for cosmology and stellar evolution studies. As the major source of uncertainty is due to photometric redshifts, improving their accuracy will be a priority. Graham et al. (2020) demonstrated that adding near-infrared and near-ultraviolet photometry from the Euclid, Wide-Field Infrared Survey Telescope (WFIRST), and/or Cosmological Advanced Survey Telescope for Optical and ultraviolet Research (CASTOR) space telescopes can reduce both the standard deviation of photometric redshift estimates and the fraction of catastrophic outliers. The combination of Rubin and Euclid data would bring significant improvements also for other transient detection systematics, in particular for the estimate of the dust extinction bias (Guy et al. 2022). A different scenario is expected for the DDF, where improvements in the photometric redshifts could certainly derive from the wealth of ancillary multi-wavelength data, with

the drawback of using a smaller area and reducing the SN statistics. Spectroscopic follow up with other facilities could also provide a good sample of galaxies properties for SN rate analysis (albeit limited to low redshift). Finally, novel deep learning techniques to measure photometric redshift have shown to outperform other methods and might also be evaluated for LSST (e.g., Pasquet et al. 2019).

We used progenitor models from Greggio (2005) as a reference and adopted the SFH from Madau & Fragos (2017) to get predicted SN Ia rates for different progenitors. We found the combination of the uncertainties analyzed in this work to be as large as the discrepancy between the rate predictions from different progenitors. However, the scatter between the rate measurements is significantly lower than that between rate measurements obtained comparing multiple surveys, thus confirming the enormous capability of LSST. It is also worth noticing that up to $z \sim 1.0$ different models have similar outcomes and it would be necessary going to higher redshift to distinguish between them. An improvement of the redshift coverage could be possibly attained through the combination of Rubin and Roman data, which is expected to detect SN Ia up to $z \sim 3$, further increasing both the dimension and the variety of the sample (Rose et al. 2021; Wang et al. 2023). Moreover, our analysis on the effect of the uncertainties is also important to measure the SN Ia rate as a function of host galaxy intrinsic colors or specific SFR (which results to be promising in separating the predictions of different models as shown in Greggio & Cappellaro 2019). Unfortunately, correlations between SN types and host galaxy properties were not included in this simulation, but their investigation is subject to subsequent analysis.

Acknowledgements. This paper has undergone internal review in the LSST Dark Energy Science Collaboration. We thank the internal reviewers Francisco Forster, Dominique Fouchez, and Christopher Frohmaier for their comments. We also deeply thank Richard Kessler for his help and advice throughout the work, especially on photometric classification and photometric redshifts. The DESC acknowledges ongoing support from the Institut National de Physique Nucléaire et de Physique des Particules in France; the Science & Technology Facilities Council in the United Kingdom; and the Department of Energy, the National Science Foundation, and the LSST Corporation in the United States. DESC uses resources of the IN2P3 Computing Center (CC-IN2P3-Lyon/Villeurbanne - France) funded by the Centre National de la Recherche Scientifique; the National Energy Research Scientific Computing Center, a DOE Office of Science User Facility supported by the Office of Science of the U.S. Department of Energy under Contract No. DE-AC02-05CH11231; STFC DiRAC HPC Facilities, funded by UK BEIS National E-infrastructure capital grants; and the UK particle physics grid, supported by the GridPP Collaboration. This work was performed in part under DOE Contract DE-AC02-76SF00515. V.P. and M.T.B. were responsible for the overall analysis and interpretation of the data, and wrote the paper. E.C. contributed to the analysis and interpretation of the results. L.G. provided theoretical models for SN Ia progenitor systems. B.O.S. provided data from his previous work and hints on the analysis. A.M. contributed to photometric classification with SuperNNova, while M.S. contributed to photometric classification with PSNID. M.L.G. provided comments on photometric redshifts and helped exploiting DPO and RSP resources. M.P. and F.B. provided final comments on the analysis and the results. All authors contributed with notes and comments to improve the clarity of the paper. A.M. is supported by the Australian Research Council Discovery Early Career Researcher Award (ARC DECRA) project number DE23010005. M.S. acknowledges support from DOE grant DE-FOA-0002424 and NSF grant AST-2108094. M.P. and V.P. acknowledge the financial contribution from PRIN-MIUR 2022 funded by the European Union – Next Generation EU, and from the Timedomes grant within the “INAF 2023 Finanziamento della Ricerca Fondamentale”. The research has made use of the following Python software packages: Astropy (Astropy Collaboration et al. 2013, 2018), Matplotlib (Hunter 2007), Pandas (van der Walt & Millman 2010), NumPy (van der Walt et al. 2011), SciPy (Virtanen et al. 2020). Other software specific for SN analysis are cited in the paper.

References

- Alard, C. & Lupton, R. H. 1998, *ApJ*, 503, 325
 Alves, C. S., Peiris, H. V., Lochner, M., et al. 2022, *ApJS*, 258, 23
 Alves, C. S., Peiris, H. V., Lochner, M., et al. 2023, *ApJS*, 265, 43
 Astropy Collaboration, Price-Whelan, A. M., Sipőcz, B. M., et al. 2018, *AJ*, 156, 123
 Astropy Collaboration, Robitaille, T. P., Tollerud, E. J., et al. 2013, *A&A*, 558, A33
 Badenes, C., Hughes, J. P., Bravo, E., & Langer, N. 2007, *ApJ*, 662, 472
 Barbary, K., Aldering, G., Amanullah, R., et al. 2012, *ApJ*, 745, 31
 Betoule, M., Kessler, R., Guy, J., et al. 2014, *A&A*, 568, A22
 Blanc, G., Afonso, C., Alard, C., et al. 2004, *A&A*, 423, 881
 Botticella, M. T., Cappellaro, E., Greggio, L., et al. 2017, *A&A*, 598, A50
 Botticella, M. T., Riello, M., Cappellaro, E., et al. 2008, *A&A*, 479, 49
 Cappellaro, E., Botticella, M. T., Pignata, G., et al. 2015, *A&A*, 584, A62
 Cappellaro, E., Botticella, M. T., Pignata, G., et al. 2016, *VizieR Online Data Catalog*, J/A+A/584/A62
 Cappellaro, E., Evans, R., & Turatto, M. 1999, *A&A*, 351, 459
 Community Engagement Team & Operations Executive Team. 2022, *Guidelines for Community Participation in Data Preview 0*, Vera C. Rubin Observatory Technical Note
 Dahlen, T., Strolger, L.-G., & Riess, A. G. 2008, *ApJ*, 681, 462
 Dhawan, S., Leibundgut, B., Spyromilio, J., & Blondin, S. 2016, *A&A*, 588, A84
 Dilday, B., Kessler, R., Frieman, J. A., et al. 2008, *ApJ*, 682, 262
 Dilday, B., Smith, M., Bassett, B., et al. 2010, *ApJ*, 713, 1026
 Foley, R. J., Simon, J. D., Burns, C. R., et al. 2012, *ApJ*, 752, 101
 Förster, F., Muñoz Arancibia, A. M., Reyes-Jainaga, I., et al. 2022, *AJ*, 164, 195
 Frohmaier, C., Sullivan, M., Nugent, P. E., et al. 2019, *MNRAS*, 486, 2308
 Gagliano, A., Narayan, G., Engel, A., Carrasco Kind, M., & LSST Dark Energy Science Collaboration. 2021, *ApJ*, 908, 170
 Graham, M. L., Bellm, E., Guy, L., et al. 2020, *LSST Alerts: Key Numbers*, Vera C. Rubin Observatory Data Management Technical Note
 Graham, M. L., Connolly, A. J., Ivezić, Ž., et al. 2018, *AJ*, 155, 1
 Graham, M. L., Connolly, A. J., Wang, W., et al. 2020, *AJ*, 159, 258
 Graur, O. & Maoz, D. 2013, *MNRAS*, 430, 1746
 Graur, O., Poznanski, D., Maoz, D., et al. 2011, *MNRAS*, 417, 916
 Graur, O., Rodney, S. A., Maoz, D., et al. 2014, *ApJ*, 783, 28
 Graur, O. & Woods, T. E. 2019, *MNRAS*, 484, L79
 Greggio, L. 2005, *A&A*, 441, 1055
 Greggio, L. 2010, *MNRAS*, 406, 22
 Greggio, L. & Cappellaro, E. 2019, *A&A*, 625, A113
 Gris, P., Regnault, N., Awan, H., et al. 2023, *ApJS*, 264, 22
 Gupta, R. R., Kuhlmann, S., Kovacs, E., et al. 2016, *AJ*, 152, 154
 Guy, J., Sullivan, M., Conley, A., et al. 2010, *A&A*, 523, A7
 Guy, L. P., Cuillandre, J.-C., Bachelet, E., et al. 2022, in *Zenodo id. 5836022*, Vol. 58, 5836022
 Hambleton, K. M., Bianco, F. B., Street, R., et al. 2023, *PASP*, 135, 105002
 Hardin, D., Afonso, C., Alard, C., et al. 2000, *A&A*, 362, 419
 Heitmann, K., Finkel, H., Pope, A., et al. 2019, *ApJS*, 245, 16
 Hochreiter, S. & Schmidhuber, J. 1997, *Neural Computation*, 9, 1735–1780
 Horesh, A., Poznanski, D., Ofek, E. O., & Maoz, D. 2008, *MNRAS*, 389, 1871
 Hunter, J. D. 2007, *Computing in Science and Engineering*, 9, 90
 Iben, I., J. & Tutukov, A. V. 1984, *ApJS*, 54, 335
 Ivezić, Ž., Kahn, S. M., Tyson, J. A., et al. 2019, *ApJ*, 873, 111
 Jones, D. O., Scolnic, D. M., Foley, R. J., et al. 2019, *ApJ*, 881, 19
 Kelly, P. L., Fox, O. D., Filippenko, A. V., et al. 2014, *ApJ*, 790, 3
 Kerzendorf, W. E., Do, T., de Mink, S. E., et al. 2019, *A&A*, 623, A34
 Kessler, R., Bernstein, J. P., Cinabro, D., et al. 2009, *PASP*, 121, 1028
 Kessler, R., Conley, A., Jha, S., & Kuhlmann, S. 2010, *arXiv e-prints*, arXiv:1001.5210
 Kessler, R., Narayan, G., Avelino, A., et al. 2019, *PASP*, 131, 094501
 Kron, R. G. 1980, *ApJS*, 43, 305
 Kuznetsova, N. V. & Connolly, B. M. 2007, *ApJ*, 659, 530
 Lasker, J. E. 2020, PhD thesis, University of Chicago
 Li, W., Leaman, J., Chornock, R., et al. 2011, *MNRAS*, 412, 1441
 Livio, M. & Mazzali, P. 2018, *Phys. Rep.*, 736, 1
 Lochner, M., Scolnic, D., Almoubayyed, H., et al. 2022, *ApJS*, 259, 58
 LSST Dark Energy Science Collaboration (LSST DESC), Abolfathi, B., Alonso, D., et al. 2021, *ApJS*, 253, 31
 LSST Science Collaboration, Abell, P. A., Allison, J., et al. 2009, *arXiv e-prints*, arXiv:0912.0201
 Madau, P. & Fragos, T. 2017, *ApJ*, 840, 39
 Maoz, D., Mannucci, F., & Brandt, T. D. 2012, *MNRAS*, 426, 3282
 Massarotti, M., Iovino, A., Buzzoni, A., & Valls-Gabaud, D. 2001, *A&A*, 380, 425
 Melinder, J., Dahlen, T., Mencia Trinchant, L., et al. 2012, *A&A*, 545, A96
 Mitra, A., Kessler, R., More, S., Hlozek, R., & LSST Dark Energy Science Collaboration. 2023, *ApJ*, 944, 212
 Möller, A. & de Boissière, T. 2020, *MNRAS*, 491, 4277

- Okumura, J. E., Ihara, Y., Doi, M., et al. 2014, PASJ, 66, 49
- O’Mullane, W. 2021, Data Preview 0: Definition and planning., Vera C. Rubin Observatory Technical Note
- O’Mullane, W., Alsayyad, Y., Chiang, H.-F., et al. 2023, Data Preview 0.2 and Operations rehearsal for DRP, Vera C. Rubin Observatory Technical Note
- Pain, R., Fabbro, S., Sullivan, M., et al. 2002, ApJ, 577, 120
- Pasquet, J., Bertin, E., Treyer, M., Arnouts, S., & Fouchez, D. 2019, A&A, 621, A26
- Perlmutter, S., Aldering, G., Goldhaber, G., et al. 1999, ApJ, 517, 565
- Perrett, K., Sullivan, M., Conley, A., et al. 2012, AJ, 144, 59
- Phillips, M. M. 1993, ApJ, 413, L105
- Pierel, J. D. R., Rodney, S., Avelino, A., et al. 2018, PASP, 130, 114504
- Riess, A. G., Filippenko, A. V., Challis, P., et al. 1998, AJ, 116, 1009
- Rodney, S. A., Riess, A. G., Strolger, L.-G., et al. 2014, AJ, 148, 13
- Rodney, S. A. & Tonry, J. L. 2010, ApJ, 723, 47
- Rose, B. M., Aldering, G., Dai, M., et al. 2021, arXiv e-prints, arXiv:2104.01199
- Sako, M., Bassett, B., Becker, A., et al. 2008, AJ, 135, 348
- Sako, M., Bassett, B., Becker, A. C., et al. 2018, PASP, 130, 064002
- Sako, M., Bassett, B., Connolly, B., et al. 2011, ApJ, 738, 162
- Salvato, M., Ilbert, O., & Hoyle, B. 2019, Nature Astronomy, 3, 212
- Sánchez, B. O., Kessler, R., Scolnic, D., et al. 2022, ApJ, 934, 96
- Schaefer, B. E. & Pagnotta, A. 2012, Nature, 481, 164
- Schmidt, S. J., Malz, A. I., Soo, J. Y. H., et al. 2020, MNRAS, 499, 1587
- Strolger, L.-G., Rodney, S. A., Pacifici, C., Narayan, G., & Graur, O. 2020, ApJ, 890, 140
- Sullivan, M., Le Borgne, D., Pritchett, C. J., et al. 2006, ApJ, 648, 868
- The PLAsTiCC team, Allam, Tarek, J., Bahmanyar, A., et al. 2018, arXiv e-prints, arXiv:1810.00001
- Tonry, J. L., Schmidt, B. P., Barris, B., et al. 2003, ApJ, 594, 1
- Tripp, R. & Branch, D. 1999, ApJ, 525, 209
- van der Walt, S., Colbert, S. C., & Varoquaux, G. 2011, Computing in Science and Engineering, 13, 22
- van der Walt, S. & Millman, J., eds. 2010, Proceedings of the 9th Python in Science Conference
- Vincenzi, M., Sullivan, M., Firth, R. E., et al. 2019, MNRAS, 489, 5802
- Virtanen, P., Gommers, R., Oliphant, T. E., et al. 2020, Nature Methods, 17, 261
- Wang, B. & Han, Z. 2012, New A Rev., 56, 122
- Wang, K. X., Scolnic, D., Troxel, M. A., et al. 2023, MNRAS[arXiv:2204.13553]
- Webbink, R. F. 1984, ApJ, 277, 355
- Whelan, J. & Iben, Icko, J. 1973, ApJ, 186, 1007
- Wiseman, P., Sullivan, M., Smith, M., et al. 2021, MNRAS, 506, 3330
- Zwicky, F. 1942, ApJ, 96, 28